https://doi.org/10.5194/ar-2026-19
Preprint. Discussion started: 3 June 2026

AEROSOL Research Discussions

In vitro toxicity of CNG exhaust gases and particles generated under varying driving conditions

Georgios Tsakonas[1], Rodopi Stamatiou[2], Ilias Vouitsis[1], Athanasios Besis[3], Athanasios Kouras[3], Daniel Deloglou[4], Eleni Papaioannou[4], Karine Elihn[5], Constantini Samara[3], Antigone Lazou[2], and Zissis Samaras[1]

[1]Mechanical Engineering Department, Aristotle University of Thessaloniki, GR 54124, Thessaloniki, Greece

[2]School of Biology, Aristotle University of Thessaloniki, Thessaloniki, GR 54124, Thessaloniki, Greece

[3]Environmental Pollution Control Laboratory, Department of Chemistry, Aristotle University of Thessaloniki, GR-54124 Thessaloniki, Greece, Greece

[4]Chemical Process and Energy Resources Institute (CPERI), Centre for Research and Technology Hellas (CERTH), 57001, Thessaloniki

[5]Department of Environmental Science, Stockholm University, SE-10691, Stockholm, Sweden

Correspondence to: Zissis Samaras (zisis@email.com)

Abstract.

Compressed natural gas vehicles are often considered a cleaner alternative to gasoline and diesel vehicles because they generally emit less particulate mass. However, their emissions of ultrafine particles and their potential biological effects remain insufficiently understood, especially for modern light-duty vehicles under realistic driving conditions. In this study, exhaust emissions from a Euro 6 compressed natural gas taxi were investigated on a chassis dynamometer using two driving cycles: a moderate real-driving cycle and a more dynamic cycle including cold-start operation. During the campaign, the vehicle exhibited two operating states: an initial rich-mixture condition associated with impaired aftertreatment performance, and a later stabilized condition. Gaseous pollutants, particle number, particle size distributions, soot mass, particle mass distribution, and deposited particle dose were measured. The nanoparticle-enriched particle fraction was chemically analysed for polycyclic aromatic hydrocarbons, nitrated and oxygenated derivatives, and water-soluble elements. In vitro toxicity was assessed using human lung epithelial cells exposed at the air–liquid interface to diluted gas phase and diluted whole exhaust. Rich-mixture operation strongly increased gaseous and particle emissions, while cold-start and dynamic driving also increased emissions under stabilized operation. The nanoparticle-enriched fraction contained low concentrations of organic compounds but substantially higher concentrations of water-soluble elements, dominated by zinc. Exposure to diluted exhaust reduced cell viability, increased membrane damage, and induced cytokine release. The gas phase alone produced measurable responses, while whole exhaust often produced stronger effects. However, differences between vehicle operating states and driving cycles were not consistent across all toxicological endpoints. These results show that the potential health relevance of compressed natural gas exhaust cannot be evaluated using particulate mass or regulated emissions alone. Even

https://doi.org/10.5194/ar-2026-19
Preprint. Discussion started: 3 June 2026

AEROSOL Research Discussions

low-mass nanoparticle emissions, together with gas-phase compounds and soluble particle-associated species, may contribute to cytotoxic and inflammatory responses.

1 Introduction

Compressed Natural Gas (CNG) is widely regarded as a cleaner alternative to gasoline and diesel, with the potential to contribute to energy security, environmental sustainability, and affordability (Himona & Poullikkas, 2025; EFI Foundation, et al., 2024). However, certain studies have indicated that CNG vehicles may produce higher nitrogen oxide (NOx) emissions (from 5% to 50% more) than gasoline vehicles, mainly due to their higher brake thermal engineering and combustion temperature (Lv et al., 2023; Rašić et al., 2017; Takeshita, 2012). Measurements on various new commercial and passenger vehicles utilizing CNG and bi-fuel systems equipped with Euro 6 technology showed significant reduction in carbon monoxide (CO) emissions from CNG vehicles when compared to gasoline vehicles while total and non-methane hydrocarbon and NOx emissions were found to be relatively comparable (Giechaskiel et al., 2022). Further, although it is true that CNG vehicles emit lower particulate mass concentration than diesel and gasoline vehicles, it seems like this is not the case for particle number concentrations. Several studies have shown that CNG vehicles emit large numbers of ultrafine particles (UFPs) and the position taken by legislation, which views CNG vehicles as particle-free, seems to raise significant concerns (Giechaskiel et al., 2019; Kontses et al., 2020; Lähde & Giechaskiel, 2021; Toumasatos et al., 2021; Xue et al., 2018).

UFPs, characterized by a diameter of less than 100 nm, raise significant concerns because of their capability to infiltrate the deeper regions of the respiratory system (Malakar et al., 2021; Vallabani et al., 2023). Their deposition can trigger inflammatory responses, oxidative stress, and other pathological processes. Additionally, UFPs have been associated with systemic effects beyond the lungs, including cardiovascular and neurological impacts (Lin et al., 2022; Schraufnagel, 2020). Toxic effects of urban UFP emissions vary considerably, mainly due to the inherent heterogeneity of the composition, shape, and size distribution of particles from different environments and emission sources (Moreno-Ríos et al., 2022; Su et al., 2024). Moreover, in the case of vehicle UFP emissions, parameters such as engine type, engine operating conditions, fuel-injection pressure, fuel type, fuel additives, and aftertreatment device traps can be important determinants for the release of toxic emissions (Claxton, 2015). Therefore, there is a growing interest in investigating the toxicity of these particles using in vitro cellular approaches. However, the difficulty in collecting sufficient nanoparticle mass becomes a limiting factor in many environments (Portugal et al., 2024; Vouitsis et al., 2023).

The majority of the existing knowledge regarding the toxicity of vehicle UFPs relates to diesel particles primarily and gasoline particles secondarily (Kęska, 2023; Vouitsis et al., 2023; Weitekamp et al., 2020). New diesel aftertreatment technologies, e.g. DOCs and DPFs, may shift in the size distribution of emitted particles toward smaller diameters (between 8 and 30 nm), and increase both their total particle number and the NO_2 content of the exhaust. Consequently, the resulting exhaust increases injury and inflammation in exposed rats, as vascular oxidative stress and endothelial dysfunction correlate

https://doi.org/10.5194/ar-2026-19
Preprint. Discussion started: 3 June 2026

with the UFPs count rather than with the mass of inhaled particles or the concentration of NO_2 (Karthikeyan et al., 2013; Kwon et al., 2020). Increasing evidence suggests that transition metals, as well as certain organic species, present in particles of gasoline direct injection (GDI) engine emissions generate ROS that may be involved in the production of undesirable respiratory symptoms (Charrier & Anastasio, 2012; Diaz et al., 2012; Maikawa et al., 2016). Emissions from port fuel injection (PFI) gasoline and methanol-fueled engines significantly increase oxidative stress, cell membrane leakage, lipid peroxidation, cell inflammation, and protein release in cultured cells, effects that can be related to cellular toxicity (Che et al., 2010; Durga et al., 2014; Tzamkiozis et al., 2010).

The understanding of the toxicity associated with CNG particle emissions remains relatively scarce. However, inflammatory processes can be caused by all types of exposures. Cells may respond to such stimuli by increasing cellular stress. The amount of cell stress that is induced depends on the composition, type and concentration of chemical compounds, such as PAHs and metals of emissions, regarding both gases and particles (Rossner et al., 2021). Exposure to PAHs appears to reduce cell viability, increase pro-inflammatory cytokine release and increase DNA damage (Besis et al., 2022), similar effects are observed in animal models as well (Tzamkiozis et al., 2010). The intensity of cellular responses varies with type of exposure and is influenced by the physicochemical properties of the exhaust and the delivered dose (Rossner et al., 2021). Most of the current knowledge is based on emissions originating from heavy-duty engines. In these studies, the mutagenic potency of CNG emissions was found to be similar to that of gasoline and diesel emissions, while the overall toxicity potency factors were generally lower for CNG (Agarwal et al., 2018; Jalava et al., 2012; Quiros et al., 2016; Seagrave et al., 2005; Turrio-Baldassarri et al., 2006). The knowledge gap is even greater when it comes to the toxicity of emissions from modern CNG light vehicles. This study aims to help address this gap through a series of cell exposures to exhaust emissions produced under simulated real-world driving conditions. The test vehicle was a Euro 6 taxi with 125,000 km mileage, considered representative of the CNG passenger car fleet in Greece. Gaseous and particulate emissions were measured on a chassis dynamometer by applying two driving cycles. Collected samples were chemically analysed for Polycyclic aromatic hydrocarbons (PAHs), nitrated PAHs (NPAHs), oxygenated PAHs (OPAHs), and water-soluble components. Toxicological responses were evaluated in A549 human lung epithelial cells exposed at the air–liquid interface to CVS-diluted gas phase and whole exhaust, using cell viability, membrane damage, and pro-inflammatory cytokine release as biological endpoints.

2 Materials and Methods

2.1 Test strategy, experimental setup, and driving cycles

The test vehicle was a Euro 6 bi-fuel light-duty vehicle used as a taxi in the urban area of Thessaloniki, Greece. The vehicle was equipped with a 1498 cm^3, 96 kW spark-ignition engine, manual transmission, a three-way catalyst (TWC), and a gasoline particle filter (GPF). At the time of testing, the vehicle had accumulated approximately 125,000 km. All measurements were performed with the vehicle operating in CNG mode. The fuel was market-quality CNG of unknown

https://doi.org/10.5194/ar-2026-19
Preprint. Discussion started: 3 June 2026

exact composition. Refuelling inside the laboratory was not possible, therefore, the vehicle was transported to a commercial CNG filling station when refuelling was required.

The experimental campaign was conducted in a chassis dynamometer test cell, where the vehicle was operated under controlled laboratory conditions while reproducing real-world driving profiles. The exact configuration is shown in schematic diagram in Figure 1. Exhaust was sampled under two conditions: untreated, directly from an extended tailpipe line and diluted by the Constant Volume Sampling (CVS) system.

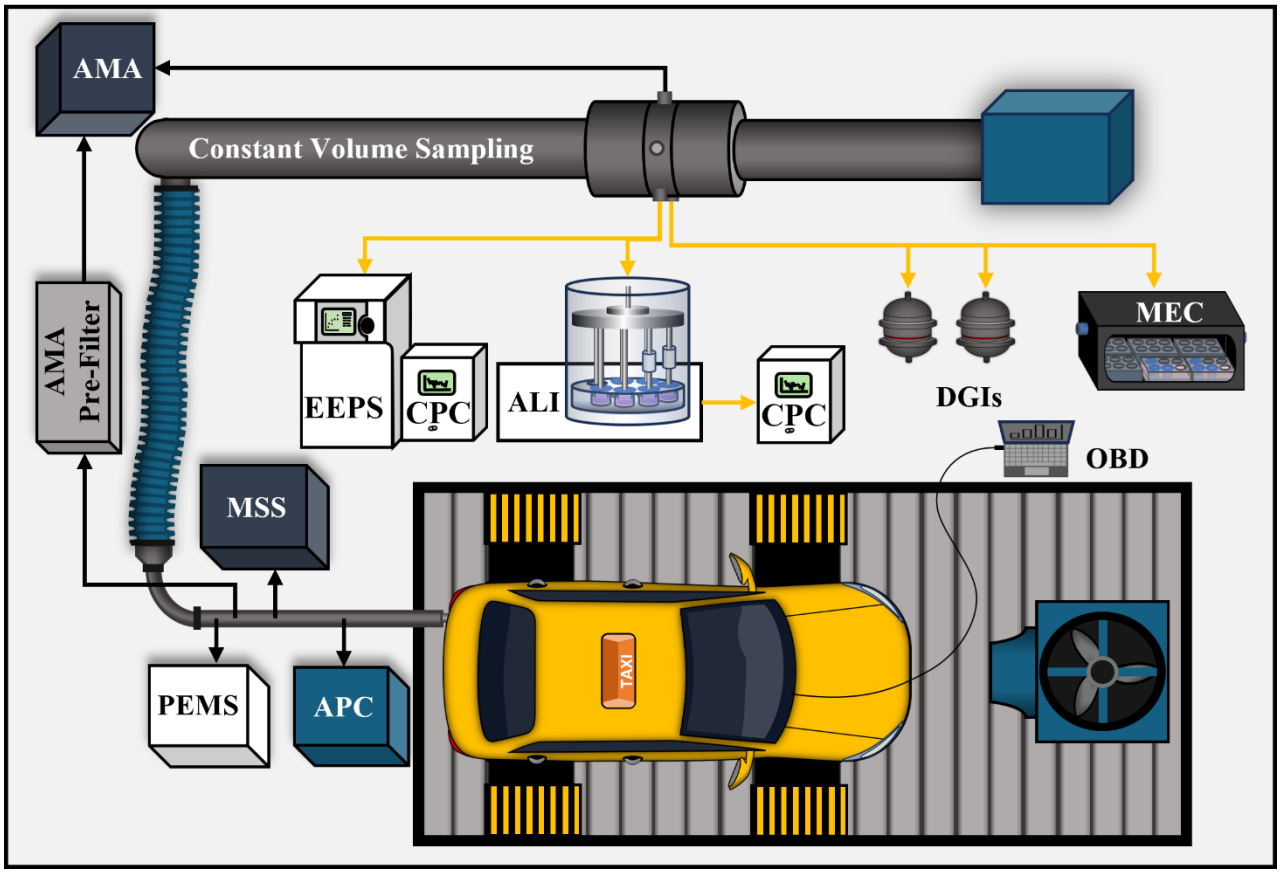

Figure 1. Experimental setup for emission measurement, particle collection, and ALI exposure of CNG exhaust.

Schematic overview of the chassis dynamometer test configuration, including direct tailpipe sampling for gaseous emissions, SPN, and soot mass measurements, and CVS-diluted exhaust sampling for particle size distribution, DGI particle mass collection, and real-time ALI exposure using the ELLIE and MEC systems.

At the direct exhaust sampling point, gaseous emissions were measured using the AMA analyser, while a Portable Emissions Measurement System (PEMS) provided real-time data of gaseous pollutants and solid particle number with a 23 nm cut-off diameter (SPN23). Solid particle number with a 10 nm cut-off diameter (SPN10) was measured using an Aerosol Particle Counter (APC), while soot mass concentration was monitored using a Micro Soot Sensor (MSS).

https://doi.org/10.5194/ar-2026-19
Preprint. Discussion started: 3 June 2026

At the CVS sampling point, diluted exhaust was used for additional particle metrics, particle mass collection and in vitro cell exposure experiments. Particle size distributions were measured using an Engine Exhaust Particle Sizer (EEPS). Total particle number with a 10 nm cut-off diameter (TPN10) was measured using Condensation Particle Counters (CPCs). For particle mass collection, two Dekati Gravimetric Impactors (DGIs) were operated in parallel at an increased flow rate of 100 L/min. This elevated flow lowered the cut-off diameter of the final impaction stage to approximately 130 nm, allowing collection of sub-130 nm particles on the backup filters, enriching the sample in nanoparticles. Due to the low particle mass emitted by the CNG vehicle, particle mass was accumulated on common filters over multiple tests rather than collected separately for each driving condition. For the toxicological assessment two ALI systems were used, one called ELectrostatic air-Liquid Interface Exposure system (ELLIE), and one Multiculture Exposure Chamber (MEC).

The vehicle was tested under two different driving scenarios. The mild Real Driving Emissions cycle (mRDE) is a chassis dynamometer reproduction of an on-road route and represents moderate real-world driving, with relatively smooth acceleration and deceleration events. The cycle covers approximately 100 km over a duration of about 2 h. The Combined Cycle (CC), more dynamic by design, integrates segments from BAB130, US06, and WLTC-low, combining high-speed, aggressive, and urban driving conditions. It covers approximately 150 km over 6950 s, corresponding to about 1 h and 55 min. The duration of both cycles was suitable for real-time cell exposure experiments. Both cycles were previously described in detail in a related study on diesel vehicle emissions (Tsakonas et al., 2025).

The experimental schedule was designed to include both cold and hot engine operation for each cycle. During the first two days of testing, when the vehicle exhibited elevated emissions associated with rich-mixture operation, the sequence consisted of a cold-start mRDE followed by a hot-start Combined Cycle. During the subsequent testing days, after the vehicle emissions stabilized, the order was reversed, with a cold-start Combined Cycle followed by a hot-start mRDE. This approach maintained the same number of cold starts and comparable total driving distance between the two operating states, allowing the effect of vehicle operation to be distinguished from the effects of driving cycle and cold-start conditions.

2.2 Chemical analysis

The particle mass accumulated on the backup filters of the DGIs was used for chemical analysis targeting PAHs, NPAHs, OPAHs, and water-soluble elements. Given the very low nanoparticle mass emissions from the vehicle, individual test cycles did not yield sufficient material for analysis. To overcome this, mass was accumulated on common backup filters across all cycles. Following collection, the filter was divided into separate portions for organic and aqueous extraction, following procedures described at Tsakonas et al. (2025).

2.2.1 Analysis of Organic Compounds (PAHs, NPAHs, OPAHs)

For the analysis of PAHs, NPAHs, and OPAHs, filter portions were extracted using microwave-assisted extraction with a mixture of dichloromethane, n-hexane, and acetone (3:2:1, v/v/v). The extraction was performed in a CEM MARSX

https://doi.org/10.5194/ar-2026-19
Preprint. Discussion started: 3 June 2026

microwave extraction unit at 110 °C and 110 psi, with a 20 min ramp time and a 10 min hold time. Before extraction, an internal standard mixture containing deuterated PAHs, NPAHs, and OPAHs was added to the samples.

The extracts were filtered, concentrated by rotary evaporation, and fractionated using a glass chromatography column packed with activated silica and sodium sulphate. PAHs were eluted with n-hexane/dichloromethane, while NPAHs and OPAHs were eluted using dichloromethane followed by acetone. The eluates were concentrated, and the NPAH/OPAH fraction was divided for separate analysis of the two compound classes.

Target compounds were quantified using gas chromatography–mass spectrometry (GC–MS; Agilent 6890N GC coupled to an Agilent 5973K MS) with a DB5-MS capillary column. PAHs, NPAHs, and OPAHs were analysed using compound-specific temperature programmes and calibration standards. Compound identification was based on the comparison of retention times and mass spectra with authentic reference standards. Procedural, method, and solvent blanks were analysed for quality control. Limits of detection and quantification were calculated using signal-to-noise ratios of 3 and 10, respectively. Surrogate recoveries were determined for all samples, and the results were not recovery corrected.

2.2.2 Analysis of Water-Soluble Elements

Filter segments intended for aqueous analysis were submerged in 5 mL of high-purity Milli-Q water and subjected to two 40-minute sonication cycles. The resulting extracts were filtered through 0.22 µm PVDF membrane filters (Millipore, USA) to remove any insoluble particles. To stabilize the samples and prevent hydrolysis, the aqueous extracts were acidified with trace metal grade HCl-HNO_3 to a final acid concentration of 2% (w/v).

The analysis included lead (Pb), barium (Ba), antimony (Sb), tin (Sn), cadmium (Cd), strontium (Sr), arsenic (As), zinc (Zn), copper (Cu), nickel (Ni), cobalt (Co), iron (Fe), manganese (Mn), chromium (Cr), vanadium (V), and aluminium (Al). The concentrations were determined using Inductively Coupled Plasma Mass Spectrometry (ICP-MS, Thermo Scientific™ iCAP™ Q). Acidified samples were introduced via peristaltic pump (40 rpm) through an autosampler and pneumatic nebulizer (Ar flow: 1.04 L/min) into a quartz spray chamber maintained at 5 °C and a concentric quartz torch with a 2.5 mm injector. Plasma generation was achieved using a 1550 W RF power source and argon gas, with ion transmission facilitated by nickel sampler and skimmer cones operating under low vacuum (1–2 mbar), and mass separation performed under high vacuum (10^{-6}–10^{-7} mbar) using a quadrupole analyser.

Calibration was performed externally using multi- and single-element standards (CPA Chem), diluted in ultrapure water and trace metal grade nitric acid. Calibration ranges were 1–1000 µg/L for Fe and 0.05–100 µg/L for most other elements. Data acquisition and instrument control were managed using Qtegra ISDS software.

2.3 Toxicological analysis

The toxicological assessment was performed using real-time ALI exposure of A549 human lung epithelial cells to diluted exhaust sampled from the CVS. ALI exposure was selected because it allows cells grown on permeable membranes to be exposed directly from the apical side to airborne gases and particles, while nutrients are supplied from the basal side. This

https://doi.org/10.5194/ar-2026-19
Preprint. Discussion started: 3 June 2026

configuration better represents inhalation exposure than conventional submerged exposure, where particles are first collected, suspended in liquid medium, and may undergo changes in size, agglomeration state, surface chemistry, or bioavailability before reaching the cells (Juárez-Facio et al., 2025; Latvala et al., 2016).

Two ALI exposure systems were used, ELLIE and MEC. ELLIE is a mobile ALI system optimized for the deposition of fine and nanosized particles and for exposure studies under realistic aerosol conditions (Juárez-Facio et al., 2025). MEC is a dose-controlled multiculture exposure chamber developed for efficient delivery of airborne and engineered nanoparticles to cell cultures, including diesel soot and other nanoparticle aerosols (Asimakopoulou et al., 2013). The use of both systems allowed the toxicological response to CNG exhaust to be evaluated under two complementary aerosol delivery and particle deposition configurations.

2.3.1 ALI exposure systems

In the ELLIE system, the aerosol flow is directed perpendicularly toward the cell surface and particle deposition is enhanced by electrostatic forces. Before entering the exposure module, the aerosol passed through a cyclone to remove particles larger than 2.5 µm, followed by a custom-made impactor with a 450 nm cut-off at 1.5 L/min. This configuration allowed the exposure to focus on the fine and nanosized particle fraction. Particles were charged using a radioactive ^63Ni source, and an alternating electrostatic field of ±1 kV was applied between the aerosol inlet and the electrode below the exposure chamber to enhance deposition onto the cells. This operating principle has been previously optimized for airborne nanoparticle exposure and shown to increase deposition efficiency while maintaining cell viability under controlled exposure conditions (Juárez-Facio et al., 2025; Latvala et al., 2016, 2017).

The ELLIE exposure module consists of seven chambers. The aerosol flow through each chamber was controlled by critical orifices at 214 mL/min, corresponding to a total system flow of 1.5 L/min. The aerosol was conditioned before exposure, and the exposure unit was maintained at 37 °C and high relative humidity to preserve cell viability during ALI exposure (Juárez-Facio et al., 2025). During each experiment, selected chambers were supplied with whole exhaust, containing both gases and particles, while other chambers received particle-filtered exhaust using DIF-LN40 filters. This allowed direct comparison between exposure to the gas phase alone and exposure to the combined gas-particle exhaust mixture. Particle number concentration was measured upstream and downstream of the exposure module using CPCs, enabling estimation of the particle fraction deposited in the system.

The MEC system was used as a complementary ALI exposure platform. In contrast to ELLIE, the MEC delivers the aerosol flow parallel to the cell culture surface, a configuration designed to provide continuous and relatively uniform exposure of multiple cell cultures to airborne particles. Particle deposition in this configuration is mainly governed by diffusion and inertial impaction under controlled flow conditions. The MEC design allows simultaneous exposure of multiple cell culture wells under the same aerosol atmosphere, thereby increasing the number of replicates that can be exposed during a single experiment. The system was developed as a dose-controlled exposure chamber and has been validated for efficient nanoparticle delivery. Previous characterization showed an average inner particle collection efficiency of approximately

https://doi.org/10.5194/ar-2026-19
Preprint. Discussion started: 3 June 2026

82%, while the cell-specific deposition efficiency was estimated at approximately 35%, because only part of the deposited particles reaches the cell growth area. Particle deposition and exposure uniformity were further demonstrated by TEM, fluorescence microscopy, and flow-visualization experiments (Asimakopoulou et al., 2013). Before entering the MEC system, the aerosol passed through an internal inertial separation section with an approximate cut-off diameter of 1 µm. The flow accelerates through a constriction and then changes direction sharply, causing particles larger than approximately 1 µm to impact and be removed from the flow. Therefore, MEC exposure was limited to the submicron fraction of the CVS-diluted exhaust.

Unlike ELLIE, MEC was used for whole-exhaust exposure rather than for separate comparison of particle-filtered and particle-containing exhaust. Therefore, the two systems provided complementary information: ELLIE enabled separation of gas-phase and gas-plus-particle effects, while MEC enabled parallel whole-exhaust exposure of multiple cell culture wells under a different flow and deposition principle. This comparison was important for assessing whether the observed toxicological responses were consistent across different ALI exposure configurations. In this study, "whole exhaust" refers to CVS-diluted exhaust containing both gas-phase compounds and particles, while "gas phase" refers to the same diluted exhaust after particle removal by filtration.

2.3.2 Cell culture and exposure protocol

A549 human alveolar epithelial adenocarcinoma cells were used as the in vitro respiratory cell model. This cell line is widely used as a reproducible human alveolar epithelial model for evaluating cytotoxicity, oxidative stress, and inflammatory responses to inhaled or particle-associated pollutants (Guo et al., 2021; Latvala et al., 2016; Shahzadi et al., 2023).

The cells were cultured on inserts (Falcon® Permeable Support for 6-well Plate with 0.4 µm Transparent PET Membrane) for 24h at a density of 2×10^5 cells/insert, in 5% CO_2, 37°C, with DMEM-High glucose (Gibco, Invitrogen), supplemented with 10% FBS (Fetal Bovine Serum, Gibco, Invitrogen) and 1% PS (Penicillin Streptomycin, Gibco, Invitrogen). Prior to transporting the cells to the exposure site, the medium on top of the cells in the inserts was removed and 25 mM HEPES was added in the basal medium. All exposures lasted 2h, and a negative control, meaning cells that were not exposed to emissions, remained in the incubator.

Exposed cells remained in the incubator for 24h before cell viability was assessed using Alamar Blue staining (AlamarBlueTM HS. Invitrogen). The staining solution was added to the cell culture medium and incubated for 3h. The absorbance of the resulting colored product was then measured with a photometer at 570 nm (Fluorostar, Omega, BMG), using the type:

$$Cell\ viability\ (\%) = \frac{Absorbance\ of\ exposed\ sample}{Average\ absorbance\ of\ incubator\ control} \times 100, \quad (1)$$

Cytotoxicity was evaluated by measuring the release of LDH in the culture medium during the 2h of exposure. The CyQUANT™ LDH Cytotoxicity Assay Kit (Thermo Scientific) was used. Cells treated with 10% Triton-X100 were used as a positive control, in order to have the maximum amount of LDH that can be produced by the specific type and number of

https://doi.org/10.5194/ar-2026-19
Preprint. Discussion started: 3 June 2026

cells. A negative control of unexposed cells was also used, representing the minimum amount of LDH release. Absorbance was measured at 490 nm, with background correction at 680 nm.

The cell stress induction was evaluated by cytokine release assessment. More specifically, TNF-α and IL-1β concentration in the exposure medium was evaluated using ELISA kits according to the manufacturer's instructions (MABTECH). A standard curve with known amounts of each cytokine was used for concentration evaluation.

Statistical analysis was performed using one-way ANOVA. Values are presented as mean ± standard error of the mean (SEM), and differences were considered statistically significant at $p < 0.05$.

3 Results and discussion

The main objective of this study was to assess the toxicity of particle emissions from a light-duty CNG vehicle representative of the city's modern fleet. Therefore, we selected a Euro 6 taxi with substantial mileage and an exhaust aftertreatment system that has not undergone any intervention or maintenance throughout the use of the vehicle. These vehicles have spark ignited stoichiometric ("rich burn") CNG engines with TWC and GPF as aftertreatment systems and are known for having low emissions of NOx, CO, unburned hydrocarbons (THCs) and particles. However, such performance is only achieved when the engine operates within a narrow air-fuel equivalence ratio range (λ or "lambda"), which is necessary for the TWC to effectively reduce NOx and CO emissions (Di Maio et al., 2019; Sundermann et al., 2024).

During the test campaign, we observed a significant surge in emissions during the first two days. This behaviour was linked to extended operation with a rich air-fuel mixture, which we attribute to the vehicle's continuous use in urban driving prior to testing. Under these conditions, the TWC could not operate within its optimal window, leading to elevated gaseous emissions. The lack of oxygen also prevented soot oxidation, causing particulate matter to accumulate and gradually obstruct the filter pathway. After prolonged highway driving on day 1, the engine management system adjusted λ toward stoichiometric conditions. This restored TWC efficiency, drastically reducing gaseous emissions and increasing oxygen availability, which in turn promoted soot oxidation in the GPF. The accumulated soot was then released in a series of blow-off events during test day 2. Following these events, emissions stabilized during the subsequent test days.

We decided to retain the data from the initial two days of testing, as they represent a worst-case scenario with respect to both gaseous and particulate emissions. Including this period allowed us to contrast conditions of impaired aftertreatment efficiency with those of normal stoichiometric operation. For this reason, the results are presented in two groups, hereafter referred to as untuned operation (day 1 and 2) and tuned operation (rest of the days), in order to investigate whether differences in engine management and aftertreatment performance translate into measurable variations in the toxicity of the emitted particles.

https://doi.org/10.5194/ar-2026-19
Preprint. Discussion started: 3 June 2026

3.1 Gaseous and particle emissions

Figure 2 presents THC/CH_4, CO, NOx, and soot mass emissions for the tested vehicle, including the average values under untuned and tuned operation, as well as the individual hot mRDE and cold Combined cycle results that constitute the tuned-operation dataset. Under untuned operation, all gaseous emissions were substantially higher than the tuned-operation average. CO emissions exceeded 1000 mg/km and were approximately six times higher than the average measured under tuned operation. The differences in THC/CH_4 and NOx emissions, although less pronounced than for CO, were still considerable, showing increases of approximately 120% and 165%, respectively.

It is important to note that the measurement schedule was balanced between the two operating conditions. During the first two days, corresponding to untuned operation, two tests were conducted each day: a cold-start mRDE followed by a hot-start Combined Cycle. During the following test days, corresponding to tuned operation, the order was reversed, with a cold-start Combined Cycle followed by a hot-start mRDE. In this way, the daily distance covered, the driving dynamics, and the number of cold starts were kept comparable between the two operating states. Therefore, the observed differences cannot be attributed to the test design, but mainly to the vehicle operating mode.

Under tuned operation, the vehicle behaved as expected for a modern Euro 6 CNG car, with low gaseous emissions across both cycles. This highlights the strong dependence of TWC efficiency on stoichiometric operation and confirms that the elevated emissions during untuned operation were the direct result of rich-mixture conditions. Notably, within the tuned-operation dataset, the individual cycle results show that the cold-start Combined Cycle produced higher gaseous emissions than the hot mRDE cycle, with increases of approximately 108% for CO, 300% for THC/CH_4, and 108% for NOx. These findings underline the combined influence of engine calibration, cold-start operation, and driving dynamics on gaseous pollutant levels.

https://doi.org/10.5194/ar-2026-19
Preprint. Discussion started: 3 June 2026

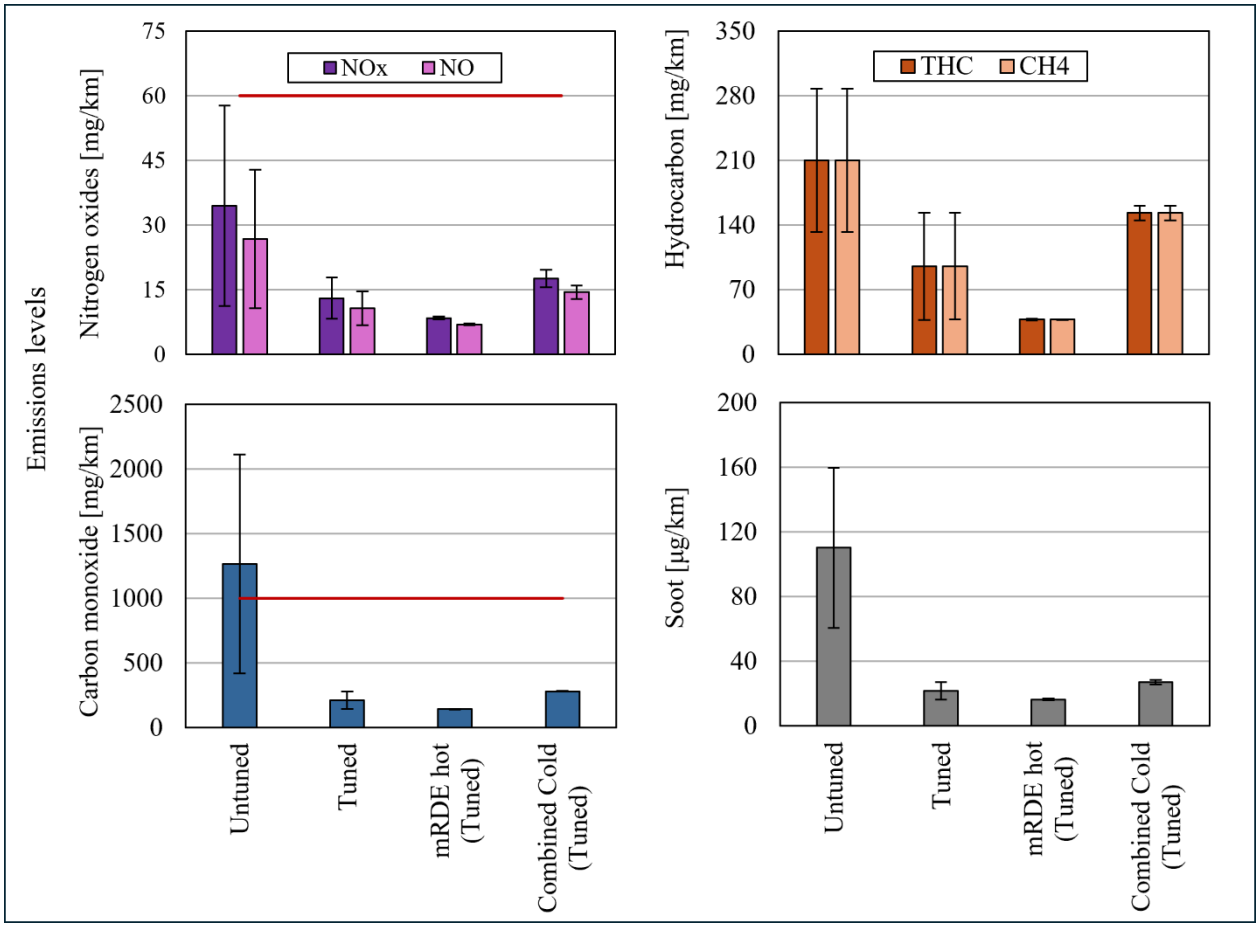

Figure 2. Gaseous and soot mass emissions under tuned and untuned CNG vehicle operation. Average THC/CH_4, CO, NOx, and soot mass emissions are shown for untuned and tuned operation, together with the individual hot mRDE and cold Combined Cycle results included in the tuned-operation dataset. Red lines indicate the WLTC reference legislative limits for CO (1000 mg/km) and NOx (60 mg/km).

The deterioration observed during untuned operation was also reflected in particle emissions. Soot mass emissions were approximately five times higher under untuned operation than the tuned-operation average. Within the tuned-operation dataset, the cold-start Combined Cycle resulted in approximately 65% higher soot mass emissions than the hot mRDE cycle, demonstrating the influence of driving cycle and engine temperature on particulate mass emissions.

A similar trend was observed for particle number emissions, as shown in Figure 3. Particle number emissions during untuned operation were markedly higher than the tuned-operation average across all particle size cut-offs and particle metrics, with increases of approximately 90% for SPN23, 110% for SPN10, and up to 700% for TPN. Within the tuned-operation dataset, PN emissions from the cold-start Combined Cycle exceeded those from the hot mRDE cycle by approximately 160%, 280%, and 960% for SPN23, SPN10, and TPN, respectively.

https://doi.org/10.5194/ar-2026-19
Preprint. Discussion started: 3 June 2026

Taken together, the gaseous and particle emission results highlight two main points. First, untuned operation, linked to rich combustion and impaired aftertreatment performance, led to a sharp increase in both gaseous and particulate emissions. Second, even under tuned operation, cold-start conditions and the more dynamic Combined cycle strongly affected particle emissions, particularly for smaller particle size cut-offs.

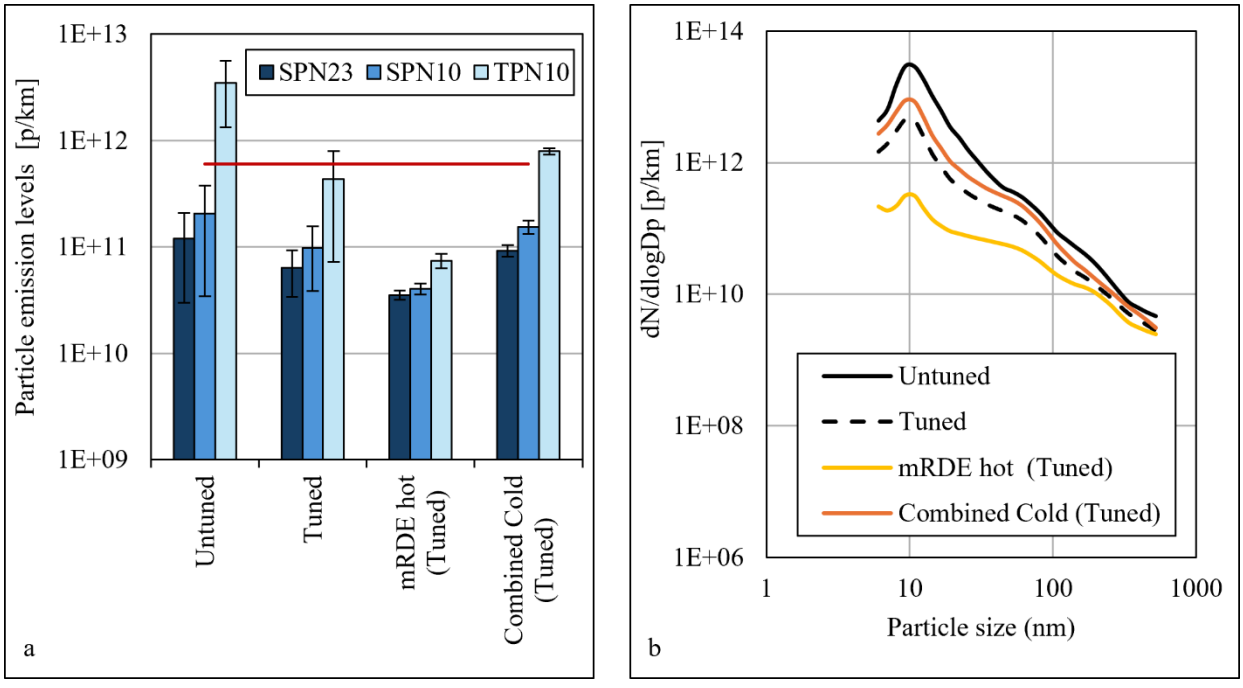

Figure 3. Particle number emissions (a) and particle size distributions (b) under tuned and untuned CNG vehicle operation.

SPN23, SPN10, and TPN10 emissions are shown for untuned and tuned operation, together with the individual hot mRDE and cold Combined Cycle results included in the tuned-operation dataset. Particle size distributions are presented for the tested operating and driving conditions. Red lines indicate the WLTC reference legislative limits for SPN23 (6×10^{11} p/km).

The particle size distributions obtained under both tuned and untuned operation, and across all test cycles, displayed a broadly similar shape despite the large differences in total particle concentration. This suggests that the main particle formation mechanisms remained comparable between conditions, while their intensity varied substantially. Across the distributions, three particle modes could be distinguished qualitatively: a nucleation mode peaking around 10 nm, a second mode centred around 50 nm, and a larger mode slightly above 100 nm. The smallest mode is consistent with freshly formed nucleation particles, while the intermediate mode may reflect accumulation-mode particles formed by condensation and coagulation processes. The larger mode is likely associated with agglomerated soot or particles released from the GPF. The presence of bi- or trimodal particle size distributions has also been reported for PAH-associated particles in exhaust emissions (Yang et al., 2005), suggesting that organic species may contribute to the observed PSD structure.

Figure 4 links the physical characterization of the emitted particles with the subsequent chemical and toxicological analyses. The DGI mass distribution shows that most of the collected particle mass was found in the intermediate impactor stages,

https://doi.org/10.5194/ar-2026-19
Preprint. Discussion started: 3 June 2026

while the backup-filter fraction below approximately 130 nm represented a smaller but analytically relevant nanoparticle-enriched fraction used for chemical characterization. In parallel, the deposited-dose results show that measurable particle mass reached the cell cultures during ALI exposure, supporting the relevance of the toxicological assessment despite the low overall particle mass emitted by the CNG vehicle. Therefore, the chemical profile obtained from the DGI backup filters and the biological responses observed in the ALI systems should be interpreted as complementary information on the nanoparticle-enriched fraction of the CVS-diluted exhaust.

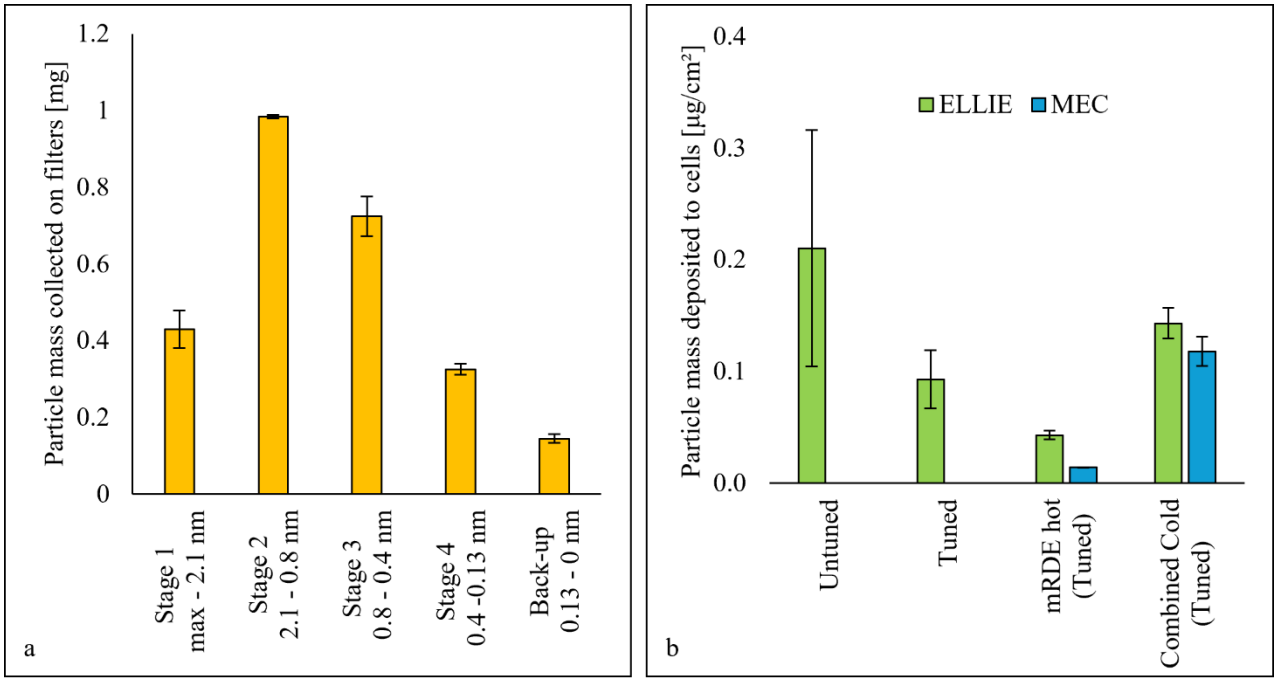

Figure 4. Particle mass distribution and deposited particle dose during CNG exhaust exposure.

Panel (a) shows the particle mass collected in the DGI stages and backup filter, representing the aerodynamic particle mass distribution of the CVS-diluted CNG exhaust. Panel (b) shows the estimated deposited particle dose during ALI exposure in the ELLIE and MEC systems.

The deposited-dose results also indicate that the relative behaviour of the two ALI systems depended on the driving condition. During the hot mRDE cycle, MEC showed a substantially lower deposited particle mass than ELLIE, whereas during the cold Combined Cycle the deposited doses in the two systems were more comparable. This difference is likely related to changes in the particle size distribution between the two cycles. The Combined Cycle produced a larger fraction of very small particles, for which deposition in the MEC system may be more efficient than for larger particle sizes, while ELLIE maintained high deposition efficiency through electrostatic enhancement. Thus, the deposited dose was influenced not only by the emitted particle mass, but also by the size distribution and the deposition principle of each ALI system.

https://doi.org/10.5194/ar-2026-19
Preprint. Discussion started: 3 June 2026

AEROSOL Research Discussions

3.2 Particle mass chemical characterisation

Particle mass for chemical analysis was collected on the DGI backup filters, corresponding to the nanoparticle-enriched fraction below approximately 130 nm. Because of the low particle mass emitted by the CNG vehicle, the filters were collected across all driving conditions and therefore represent an integrated chemical profile of the emitted nanoparticle fraction rather than cycle-specific composition. Since both the DGI sampling and the ALI exposure systems received diluted exhaust from the CVS, the chemical profile obtained from the backup filters is directly relevant to the particle fraction to which the cells were exposed, at least for particles smaller than 130 nm.

3.2.1 Organic analysis

Figure 5 presents the concentrations and relative contributions of the analysed PAHs, NPAHs, and OPAHs in the nanoparticle-enriched particle fraction. The total concentrations of ∑16PAHs, ∑8OPAHs, and ∑7NPAHs were 0.81, 0.24, and 0.07 ng/m^3, respectively, following the order PAHs > OPAHs > NPAHs.

The PAH profile was dominated by low-molecular-weight compounds, mainly naphthalene (NAP, 53%), phenanthrene (PHE, 15%), and pyrene (PYR, 13%), which together accounted for approximately 81% of the total PAH concentration. The remaining PAH fraction was mainly represented by fluoranthene (FLT, 7%), anthracene (ANT, 3%), acenaphthylene (ACY, 2%), fluorene (FLN, 2%), acenaphthene (ACE, 1%), and chrysene (CHR, 1%), while the heavier PAHs each contributed less than 1%.

For NPAHs, 1-nitronaphthalene (1-NNAP, 34%), 2-nitronaphthalene (2-NNAP, 36%), and 1-nitropyrene (1-NPYR, 19%) were the dominant species, together contributing approximately 89% of the total NPAHs. The remaining NPAH fraction was composed of 5-nitroacenaphthene (5-NACE, 4%), 3-nitrobiphenyl (3-NBP, 4%), 4-nitrobiphenyl (4-NBP, 1%), and 2+3-nitrofluoranthene (2+3-NFLT, 1%).

Similarly, the OPAH fraction was mainly composed of 1,4-naphthoquinone ((1,4)O_2NAP, 36%), 9-fluorenone (9-OFLN, 30%), and acenaphthoquinone (AceNQ, 22%), which together accounted for approximately 88% of the total OPAHs. The remaining OPAHs included 9,10-anthraquinone ((9,10)O_2ANT, 7%), 2-nitrofluorenone (2-N-9-OFLN, 2%), 1,2-benzanthraquinone (1,2-O_2BAA, 2%), benzanthrone (BAN, 2%), and benzo[a]fluorenone (BaOFLN, <1%).

Although NPAHs and OPAHs were present at lower absolute concentrations than parent PAHs, their presence is relevant because these derivatives are often associated with oxidative and inflammatory responses.

https://doi.org/10.5194/ar-2026-19
Preprint. Discussion started: 3 June 2026

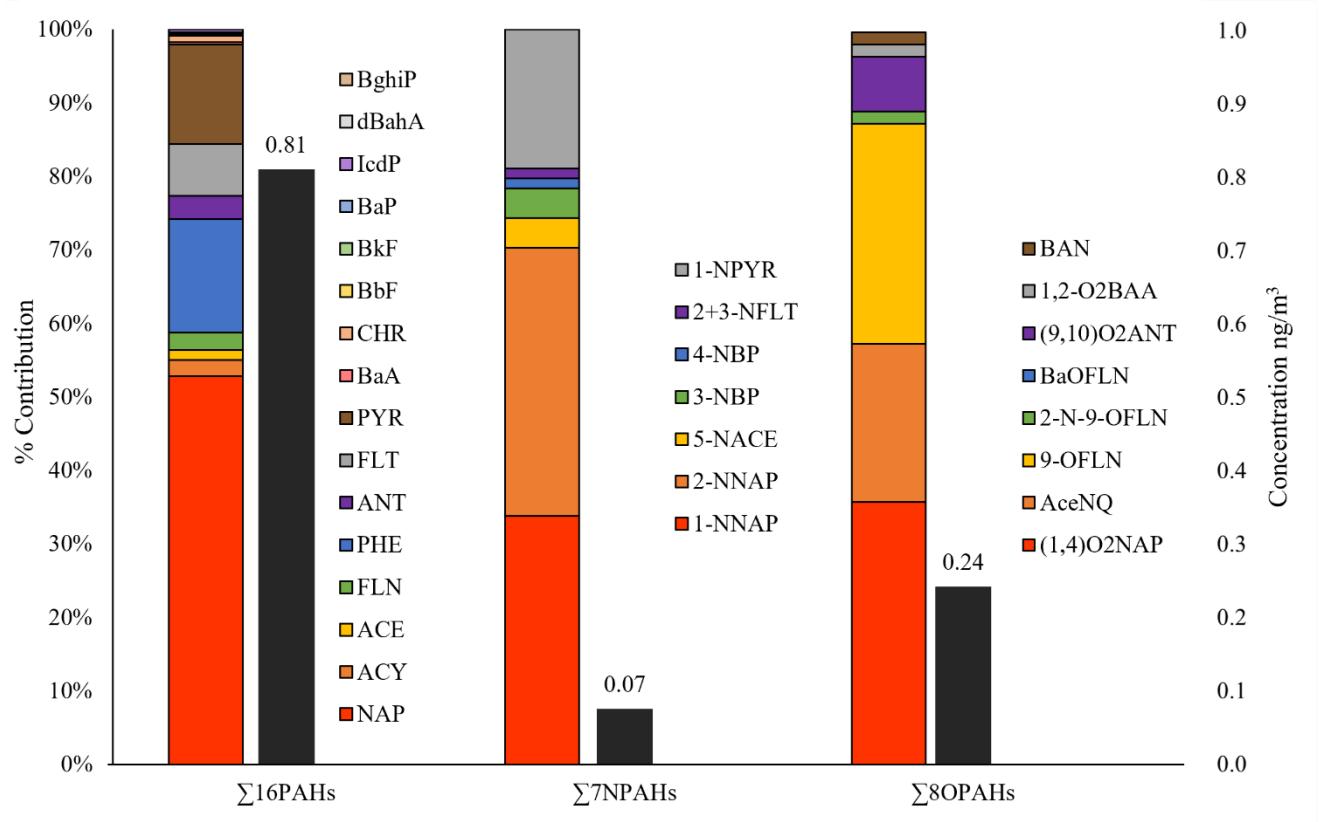

Figure 5. Organic chemical profile of nanoparticle-enriched particles emitted by the CNG vehicle.

Relative contributions and concentrations of PAHs, NPAHs, and OPAHs measured in the DGI backup-filter samples, corresponding to particles below approximately 130 nm. Samples were collected from CVS-diluted exhaust across all driving conditions and therefore represent an integrated organic profile of the emitted nanoparticle-enriched fraction.

3.2.2 Inorganic analysis

Figure 6 presents the concentrations and relative contributions of the analysed water-soluble elements in the nanoparticle-enriched particle fraction. Water-soluble elements were detected at substantially higher concentrations than the analysed organic compounds, with a total concentration of 21.5 ng/m^3.

The elemental profile was strongly dominated by zinc (Zn), which reached 18 ng/m^3 and accounted for approximately 85% of the total measured water-soluble elements. Aluminium (Al, 7%) and iron (Fe, 4%) were the next most abundant elements, while the remaining elements each contributed 1% or less. Together, Zn, Al, and Fe accounted for approximately 96% of the quantified water-soluble elemental fraction. The remaining fraction was mainly represented by manganese (Mn, 1%), nickel (Ni, 1%), antimony (Sb, 1%), and barium (Ba, 1%), while copper (Cu), strontium (Sr), tin (Sn), chromium (Cr), cobalt (Co), and lead (Pb) each contributed less than 1%; vanadium (V), arsenic (As), and cadmium (Cd) were below the limit of

https://doi.org/10.5194/ar-2026-19
Preprint. Discussion started: 3 June 2026

detection. This indicates that the water-soluble inorganic fraction was a major component of the chemically characterized nanoparticle mass and that Zn was the dominant water-soluble element in the collected CNG particle sample.

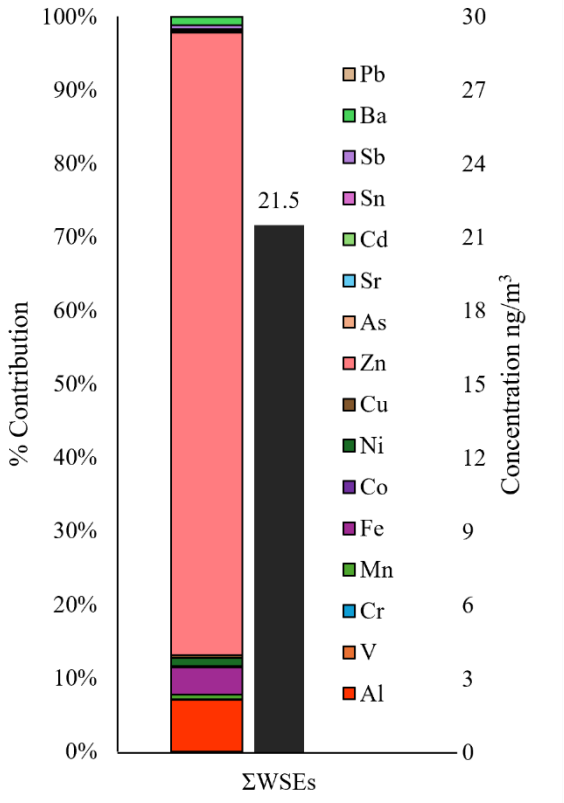

Figure 6. Water-soluble elemental profile of nanoparticle-enriched particles emitted by the CNG vehicle.

Relative contributions and concentrations of water-soluble elements measured in the DGI backup-filter samples, corresponding to particles below approximately 130 nm. Samples were collected from CVS-diluted exhaust across all driving conditions and therefore represent an integrated inorganic profile of the emitted nanoparticle-enriched fraction.

3.3 Toxicological characterization

The toxicological response of A549 cells exposed to CVS-diluted CNG exhaust was evaluated through cell viability, LDH release, and cytokine production. Figure 7 presents the comparison between tuned and untuned vehicle operation for all endpoints. Exposure to both gas phase and whole exhaust reduced cell viability and increased LDH release compared with the respective controls. However, the differences between tuned and untuned operation were not consistent across these cytotoxicity-related endpoints, indicating that the change in vehicle operating state did not translate into a clear difference in cell viability or membrane damage.

A stronger indication of an effect of vehicle operation was observed for the inflammatory endpoints. IL-1β and TNF-α release increased after exposure, and the response tended to be higher for whole exhaust under untuned operation, particularly for cytokine production. Nevertheless, these differences should be interpreted cautiously, since they were not

https://doi.org/10.5194/ar-2026-19
Preprint. Discussion started: 3 June 2026

consistently significant across all comparisons. Overall, the tuned–untuned comparison suggests that both operating states induced measurable biological responses, with some indication that untuned whole exhaust may enhance inflammatory signalling.

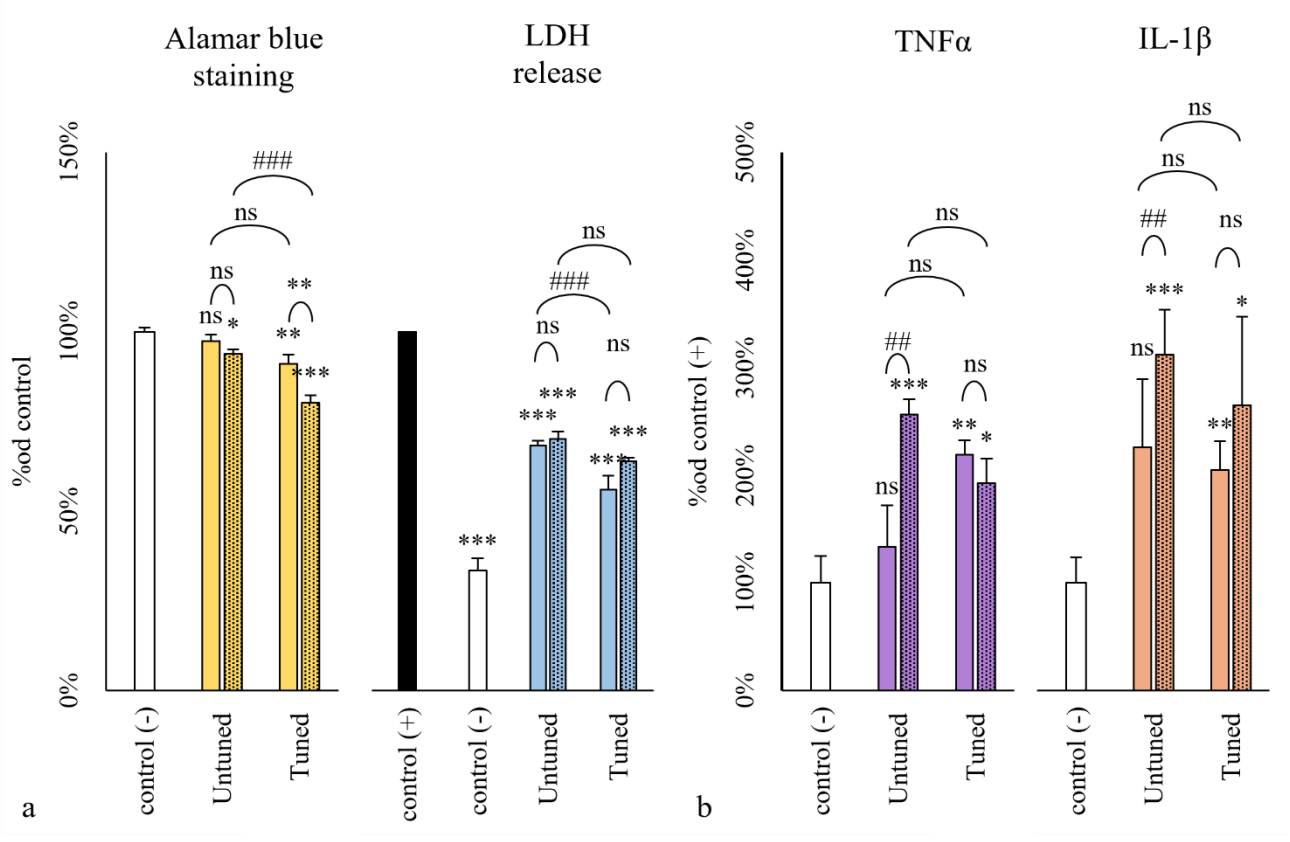

Figure 7. Toxicological responses under tuned and untuned CNG vehicle operation.

Comparison of A549 cell responses after exposure to CVS-diluted gas phase and whole exhaust under tuned and untuned operation. Panel (a) cell viability assessed by Alamar Blue staining and cytotoxicity assessed by LDH release. Panel (b) shows cytokine release, including TNF-α and IL-1β. *p<0.05, **p < 0.01, ***p<0.0001, compared to control, One Way ANOVA. #p<0.05, ##p < 0.01, ###p<0.0001, intercomparison of exposure conditions, One Way ANOVA

Figure 8 also includes the corresponding MEC results for cell viability and LDH release under whole-exhaust exposure. Since MEC was used only for whole-exhaust exposure, the most appropriate comparison between systems is with the whole-exhaust conditions in ELLIE. Both systems showed reduced viability and increased LDH release after exposure, although the magnitude of the response differed between systems. These differences are expected, given the different aerosol delivery, flow configuration, and particle deposition mechanisms of ELLIE and MEC.

https://doi.org/10.5194/ar-2026-19
Preprint. Discussion started: 3 June 2026

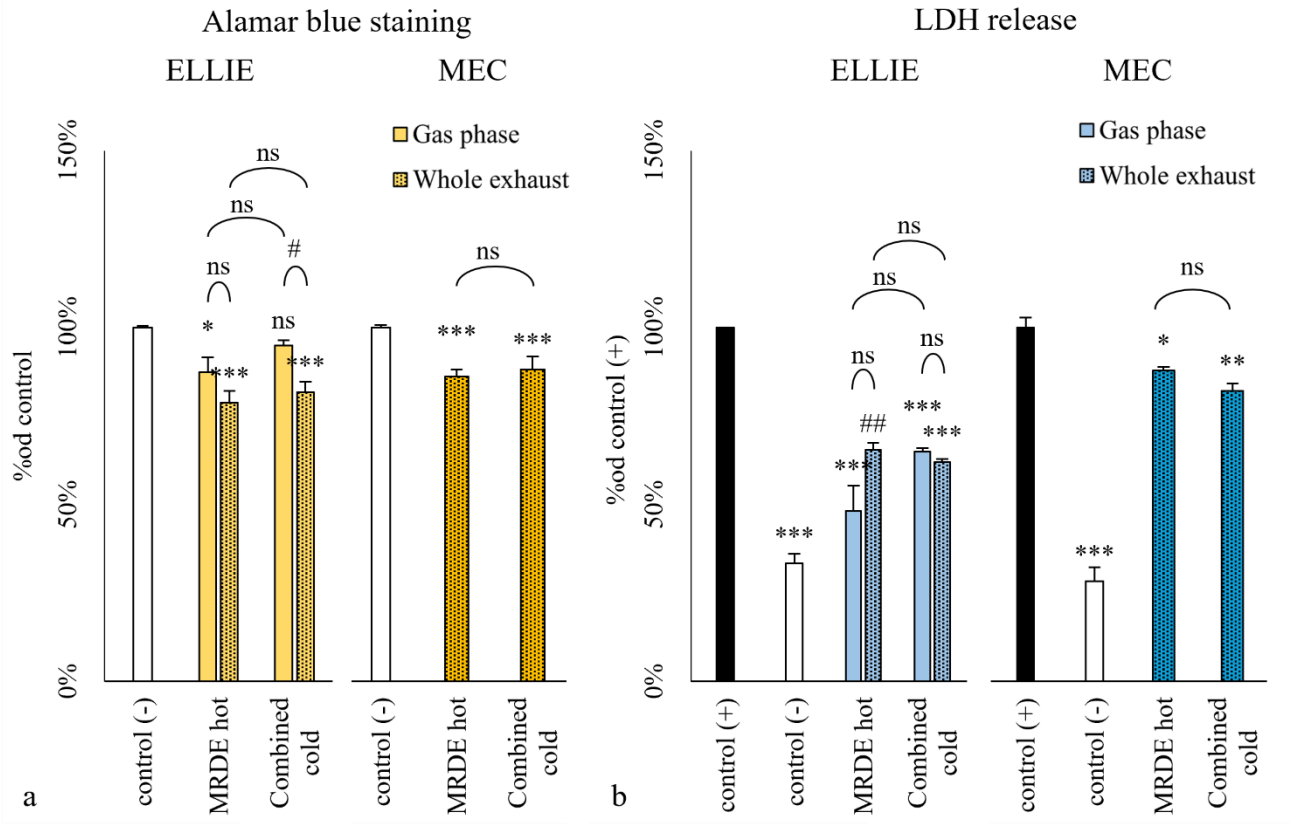

Figure 8. Cell viability and cytotoxicity under tuned operation: comparison of driving conditions and ALI exposure systems.

Comparison of A549 cell responses after exposure to CVS-diluted gas phase and whole exhaust during the hot mRDE and cold Combined Cycle under tuned operation. Responses obtained with the ELLIE and MEC exposure systems are shown where applicable. Panel (a) shows cell viability assessed by Alamar Blue staining. Panel (b) shows cytotoxicity assessed by LDH release. *p<0.05, **p<0.01, ***p<0.0001, compared to control, One Way ANOVA. #p<0.05, ##p<0.01, ###p<0.0001, intercomparison of exposure conditions, One Way ANOVA.

Cytokine release under tuned operation is presented in Figure 9. Both IL-1β and TNF-α increased after exposure, confirming the induction of a pro-inflammatory response. For IL-1β, the cold Combined Cycle whole-exhaust exposure produced a stronger response than the corresponding gas-phase exposure and the hot mRDE exposure in the ELLIE system, suggesting that driving dynamics and/or cold-start conditions may influence the inflammatory potential of the emitted particles. This was the clearest indication that the driving condition affected the toxicological outcome. For TNF-α, the differences between driving conditions were less pronounced and did not show the same clear pattern.

The MEC results in Figure 9 also showed increased cytokine release after whole-exhaust exposure, but the pattern between the hot mRDE and cold Combined Cycle was not identical to that observed in ELLIE. Therefore, the comparison between the two ALI systems should be interpreted as complementary rather than directly interchangeable. Both systems support the

https://doi.org/10.5194/ar-2026-19
Preprint. Discussion started: 3 June 2026

conclusion that diluted CNG exhaust can induce inflammatory responses, but the magnitude and detailed pattern of the response depend on the exposure system and endpoint considered.

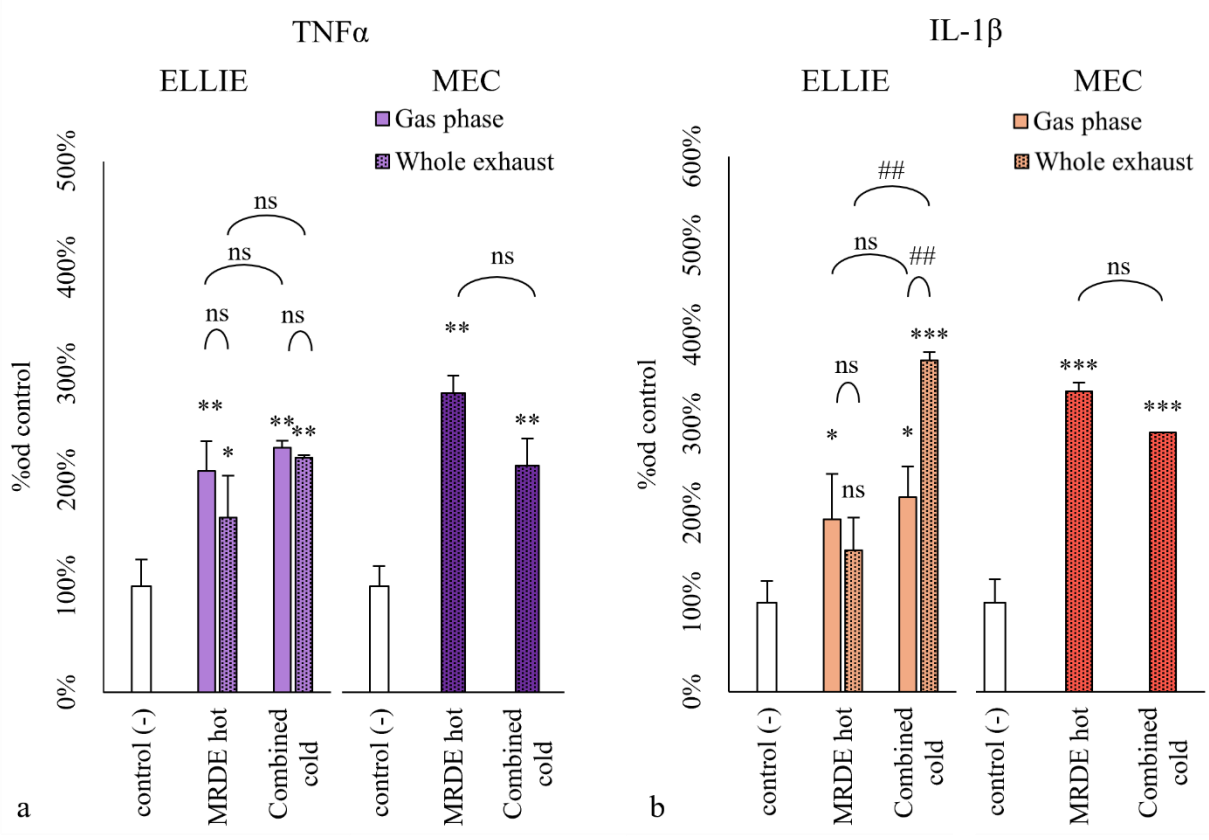

Figure 9. Cytokine release under tuned operation: comparison of driving conditions and ALI exposure systems.

Comparison of A549 inflammatory responses after exposure to CVS-diluted gas phase and whole exhaust during the hot mRDE and cold Combined Cycle under tuned operation. Responses obtained with the ELLIE and MEC exposure systems are shown where applicable. Panel (a) shows TNF-α release. Panel (b) shows IL-1β release. *p<0.05, **p<0.01, ***p<0.0001, compared to control, One Way ANOVA. #p<0.05, ##p<0.01, ###p<0.0001, intercomparison of exposure conditions, One Way ANOVA.

Overall, the toxicological results indicate that CNG exhaust affected cell viability, cytotoxicity, and inflammatory signalling in A549 cells. The gas phase alone was sufficient to induce measurable responses, while whole exhaust often produced stronger effects, highlighting the contribution of the particle-containing fraction. However, neither tuned versus untuned operation nor the comparison between hot mRDE and cold Combined Cycle produced consistently significant differences across all endpoints. Thus, the main finding is not a strong separation between operating or driving conditions, but rather that CNG exhaust, including its particle-containing fraction, can induce adverse cellular responses under the tested conditions.

https://doi.org/10.5194/ar-2026-19
Preprint. Discussion started: 3 June 2026

AEROSOL Research Discussions

4 Discussion

The present study shows that emissions from a modern Euro 6 CNG vehicle can induce measurable biological responses in lung epithelial cells, even when particle mass emissions are low. This is important because CNG vehicles are often discussed mainly in terms of reduced CO_2 and PM mass emissions compared with conventional fuels. However, our results support the view that particle number, particle size, chemical composition, and delivered dose are more informative than PM mass alone when assessing potential health relevance. Previous studies have similarly shown that CNG vehicles may emit low particle mass but substantial numbers of ultrafine particles, especially in the nucleation size range, and that the relationship between mass-based and number-based emissions can be weak (Dimopoulos Eggenschwiler et al., 2021; Jayaratne et al., 2008).

A central feature of this campaign was the contrast between two vehicle operating states. During untuned operation, the rich air–fuel mixture impaired aftertreatment performance, resulting in increased gaseous emissions and higher particle emissions. This is consistent with the known sensitivity of three-way catalysts to λ control and with previous work showing that CNG emissions can vary strongly under transient or dynamic operation (Dimaratos et al., 2019). Nevertheless, the biological response did not increase proportionally with the emission factors. This suggests that the toxicological outcome was not controlled only by the total emitted mass or number, but also by the composition of the gas phase and particle fraction, the size-dependent deposition in the ALI systems, and the specific biological endpoint considered.

The particle size distributions were broadly similar across conditions, with three apparent modes in the nucleation, intermediate, and larger particle ranges. This indicates that the same general particle formation mechanisms were probably present under both tuned and untuned operation, while their intensity changed substantially. The DGI mass distribution and deposited-dose results further help interpret this point: only a fraction of the emitted particle mass was collected in the nanoparticle-enriched backup-filter fraction used for chemical analysis, yet this fraction is directly relevant to the particles delivered to the ALI systems. The deposition results also show that exposure dose depended not only on the emitted aerosol but also on the exposure system, with ELLIE generally favouring deposition through electrostatic enhancement and MEC responding more strongly when the aerosol shifted toward smaller particle sizes.

The chemical profile of the nanoparticle-enriched fraction provides a plausible explanation for the observed biological responses. Parent PAHs were the most abundant measured organic class, followed by OPAHs and NPAHs. Although the absolute concentrations of these organic compounds were low, the presence of oxygenated and nitrated PAH derivatives is relevant because these compounds can contribute to oxidative and inflammatory responses. At the same time, the water-soluble elemental fraction was much higher than the measured organic fraction and was strongly dominated by Zn, with smaller contributions from Al and Fe. This suggests that, for this CNG vehicle, the toxicity of the nanoparticle-enriched fraction may not be driven primarily by parent PAHs alone, but by a mixed chemical profile involving soluble metals, oxygenated organics, nitrated organics, and gas-phase compounds.

The toxicological results support this mixed-exposure interpretation. Gas-phase exposure alone was sufficient to reduce cell viability, increase LDH release, and induce cytokine release, while whole exhaust often produced stronger responses. This

https://doi.org/10.5194/ar-2026-19
Preprint. Discussion started: 3 June 2026

agrees with the idea that CNG exhaust toxicity may be partly associated with gas-phase or semi-volatile compounds, not only with particles. Li et al. (2021), for example, linked toxicological responses from light-duty CNG/RNG exhaust to specific gas-phase and semi-volatile organic compounds, including benzene, dibenzofuran, formaldehyde, and other reactive species. Therefore, in the present study, the stronger responses during whole-exhaust exposure should not be interpreted as a pure "particle effect", but rather as the additional effect of a particle-containing exhaust mixture over an already active gas phase.

The cytokine pattern may also reflect the chemical nature of the exposure. TNF-α and IL-1β are regulated through partly different biological pathways: TNF-α is commonly linked to transcriptional inflammatory signalling, while IL-1β release requires both priming and post-translational processing through inflammasome-related pathways. Organic compounds such as PAHs and quinones can activate oxidative-stress-sensitive inflammatory signalling, including NF-κB-related pathways, while particles and soluble metals can contribute to lysosomal stress, mitochondrial ROS, and NLRP3 inflammasome activation (Dostert et al., 2008; Guo et al., 2021; Hornung et al., 2008; Huang et al., 2023; Øvrevik et al., 2015). In this study, the indication that IL-1β was particularly responsive under some whole-exhaust conditions is therefore compatible with a role of the particle-containing, metal-rich fraction. However, this mechanism remains inferential because ROS, caspase-1 activation, and inflammasome markers were not directly measured.

The limited separation between tuned and untuned toxicological responses is scientifically meaningful. Untuned operation clearly increased emissions, but it did not produce a uniformly stronger biological response across all endpoints. This could be due to several factors: the integrated exposure dose may not scale linearly with emission factors; the chemical composition of the biologically deposited fraction may have remained broadly similar; and the selected endpoints may respond differently to gas-phase compounds, soluble metals, and particle-associated organics. A comparable complexity has been reported in studies of diesel and dual natural gas–diesel particles, where toxicity varied with PAH and metal composition rather than with particle mass alone (Pino et al., 2025). Thus, the present results suggest that altered aftertreatment performance can strongly affect emission levels, but its effect on biological response depends on how the emitted mixture changes chemically and physically.

Overall, this work supports a cautious but important conclusion: modern CNG exhaust should not be considered toxicologically irrelevant simply because particle mass emissions are low. The gas phase and the nanoparticle-containing fraction both contributed to adverse cellular responses, while the chemical analysis points to a complex mixture of low-level organic compounds and relatively abundant water-soluble elements. The study also highlights the value of combining emission measurements, particle size distributions, deposited-dose estimates, chemical characterization, and ALI toxicology. Although the results are based on one vehicle and a limited number of biological repetitions, they show that CNG exhaust toxicity cannot be inferred from regulated emissions alone and should be evaluated using source-specific chemical and biological information.

https://doi.org/10.5194/ar-2026-19
Preprint. Discussion started: 3 June 2026

5 Conclusions

This study investigated the emissions and in vitro toxicological response of a Euro 6 bi-fuel CNG taxi tested under simulated real-world driving conditions. The vehicle exhibited two distinct operating states during the campaign: an initial untuned/rich-mixture operation associated with impaired aftertreatment performance, and a subsequent tuned/stabilized operation. This allowed the study to evaluate not only the emissions of a modern CNG light-duty vehicle, but also whether a deterioration in engine and aftertreatment operation translated into a stronger biological response. Gaseous emissions, particle number and size distributions, particle mass distribution, chemical composition of the nanoparticle-enriched fraction, deposited dose, and ALI toxicological endpoints were combined to provide an integrated assessment.

The results confirm that CNG vehicles can emit very low particle mass while still producing relevant numbers of ultrafine particles. Untuned operation caused a strong increase in both gaseous and particle emissions, while the cold and more dynamic Combined Cycle increased emissions even under tuned operation. However, the broadly similar particle size distributions across conditions suggest that the main particle formation mechanisms remained comparable, while their intensity changed.

The chemical characterization of the nanoparticle-enriched fraction showed that the collected particles contained both organic and inorganic toxicologically relevant components. PAHs were the most abundant measured organic class, followed by OPAHs and NPAHs, while water-soluble elements were present at substantially higher concentrations than the measured organics and were strongly dominated by Zn. This chemical profile suggests that the observed biological response cannot be attributed to a single compound class, but rather to a complex mixture of gas-phase compounds, particle-associated organics, and soluble inorganic species.

The toxicological results showed that CVS-diluted CNG exhaust induced measurable responses in A549 cells, including reduced cell viability, increased LDH release, and increased cytokine production. Gas-phase exposure alone was sufficient to induce biological responses, while whole exhaust often produced stronger effects, indicating that the particle-containing fraction contributed to the observed toxicity. Nevertheless, the differences between tuned and untuned operation, or between the hot mRDE and cold Combined Cycle, were not consistently significant across all endpoints. Therefore, increased emission levels did not translate linearly into stronger toxicological responses.

Overall, this work highlights that the toxicological relevance of CNG exhaust cannot be evaluated using regulated emissions or particle mass alone. Even when particle mass is low, the combination of ultrafine particles, soluble metals, oxidized/nitrated organics, and gas-phase compounds may induce cellular stress and inflammatory responses. The combined use of emission measurements, chemical characterization, deposited-dose estimation, and two ALI exposure systems provides a more complete framework for assessing the health relevance of modern CNG vehicle exhaust.

Code and data availability

The datasets generated during this study are available from the corresponding author on reasonable request.

https://doi.org/10.5194/ar-2026-19
Preprint. Discussion started: 3 June 2026

Author contributions

GT, IV, EP, and ZS contributed to the conceptualization of the study. GT, RS, IV, AB, AK, DD, EP, and KE contributed to the methodology. GT and RS performed software-related analysis. GT, RS, AB, and AK carried out the investigation, formal analysis, and data curation. GT, RS, and AB prepared the visualizations. GT and IV prepared the original draft of the manuscript. RS, AB, AK, DD, EP, KE, CS, AL, and ZS reviewed and edited the manuscript. EP, KE, CS, AL, and ZS provided resources. KE contributed to validation. AL and ZS supervised the work. ZS was responsible for project administration. KE and ZS contributed to funding acquisition.

Competing interests

The authors declare that they have no conflict of interest.

Disclaimer

Publications remains neutral with regard to jurisdictional claims made in the text, published maps, institutional affiliations, or any other geographical representation in this paper. While Copernicus Publications makes every effort to include appropriate place names, the final responsibility lies with the authors. Views expressed in the text are those of the authors and do not necessarily reflect the views of the publisher.

Financial support

This work was funded by the European Union's Horizon 2020 Research and Innovation Programme under grant agreement No. 954377 (nPETS).

References

Agarwal, A. K., Ateeq, B., Gupta, T., Singh, A. P., Pandey, S. K., Sharma, N., Agarwal, R. A., Gupta, N. K., Sharma, H., Jain, A., and Shukla, P. C.: Toxicity and mutagenicity of exhaust from compressed natural gas: Could this be a clean solution for megacities with mixed-traffic conditions?, Environmental Pollution, 239, 499–511, https://doi.org/10.1016/j.envpol.2018.04.028, 2018.

https://doi.org/10.5194/ar-2026-19
Preprint. Discussion started: 3 June 2026

Asimakopoulou, A., Daskalos, E., Lewinski, N., Riediker, M., Papaioannou, E., and Konstandopoulos, A. G.: Development of a dose-controlled multiculture cell exposure chamber for efficient delivery of airborne and engineered nanoparticles, Journal of Physics: Conference Series, 429, 012023, https://doi.org/10.1088/1742-6596/429/1/012023, 2013.

Besis, A., Gallou, D., Avgenikou, A., Serafeim, E., and Samara, C.: Size-dependent in vitro inhalation bioaccessibility of PAHs and O/N PAHs—Implications to inhalation risk assessment, Environmental Pollution, 301, 119045, https://doi.org/10.1016/j.envpol.2022.119045, 2022.

Charrier, J. G. and Anastasio, C.: On dithiothreitol (DTT) as a measure of oxidative potential for ambient particles: Evidence for the importance of soluble transition metals, Atmospheric Chemistry and Physics Discussions, 12, 11317–11350, https://doi.org/10.5194/acp-12-9321-2012, 2012.

Che, W., Liu, G., Qiu, H., Zhang, H., Ran, Y., Zeng, X., Wen, W., and Shu, Y.: Comparison of immunotoxic effects induced by the extracts from methanol and gasoline engine exhausts in vitro, Toxicology in Vitro, 24, 1119–1125, https://doi.org/10.1016/j.tiv.2010.03.008, 2010.

Claxton, L. D.: The history, genotoxicity, and carcinogenicity of carbon-based fuels and their emissions. Part 3: Diesel and gasoline, Mutation Research/Reviews in Mutation Research, 763, 30–85, https://doi.org/10.1016/j.mrrev.2014.09.002, 2015.

Di Maio, D., Beatrice, C., Fraioli, V., Napolitano, P., Golini, S., and Rutigliano, F. G.: Modeling of three-way catalyst dynamics for a compressed natural gas engine during lean–rich transitions, Applied Sciences, 9, 4610, https://doi.org/10.3390/app9214610, 2019.

Diaz, E. A., Chung, Y., Papapostolou, V., Lawrence, J., Long, M. S., Hatakeyama, V., Gomes, B., Calil, Y., Sato, R., Koutrakis, P., and Godleski, J. J.: Effects of fresh and aged vehicular exhaust emissions on breathing pattern and cellular responses – pilot single vehicle study, Inhalation Toxicology, 24, 288–295, https://doi.org/10.3109/08958378.2012.668572, 2012.

Dimaratos, A., Toumasatos, Z., Doulgeris, S., Triantafyllopoulos, G., Kontses, A., and Samaras, Z.: Assessment of CO2 and NOx emissions of one diesel and one bi-fuel gasoline/CNG Euro 6 vehicles during real-world driving and laboratory testing, Frontiers in Mechanical Engineering, 5, 62, https://doi.org/10.3389/fmech.2019.00062, 2019.

Dimopoulos Eggenschwiler, P., Schreiber, D., and Schröter, K.: Characterization of the emission of particles larger than 10 nm in the exhaust of modern gasoline and CNG light duty vehicles, Fuel, 291, 120074, https://doi.org/10.1016/j.fuel.2020.120074, 2021.

Dostert, C., Pétrilli, V., Van Bruggen, R., Steele, C., Mossman, B. T., and Tschopp, J.: Innate immune activation through Nalp3 inflammasome sensing of asbestos and silica, Science, 320, 674–677, https://doi.org/10.1126/science.1156995, 2008.

Durga, M., Nathiya, S., Rajasekar, A., and Devasena, T.: Effects of ultrafine petrol exhaust particles on cytotoxicity, oxidative stress generation, DNA damage and inflammation in human A549 lung cells and murine RAW 264.7 macrophages, Environmental Toxicology and Pharmacology, 38, 518–530, https://doi.org/10.1016/j.etap.2014.08.003, 2014.

Energy Futures Initiative (EFI) (2024). The Future of Natural Gas in a Low-Carbon World. Available at: https://efifoundation.org/reports/the-future-of-natural-gas-in-a-low-carbon-world

https://doi.org/10.5194/ar-2026-19
Preprint. Discussion started: 3 June 2026

Giechaskiel, B., Lähde, T., Clairotte, M., Suarez-Bertoa, R., Valverde, V., Melas, A. D., Selleri, T., and Bonnel, P.: Emissions of Euro 6 mono- and bi-fuel gas vehicles, Catalysts, 12, 651, https://doi.org/10.3390/catal12060651, 2022.

Giechaskiel, B., Lähde, T., and Drossinos, Y.: Regulating particle number measurements from the tailpipe of light-duty vehicles: The next step?, Environmental Research, 172, 1–9, https://doi.org/10.1016/j.envres.2019.02.006, 2019.

Guo, H., Huang, Y., Wang, H., Zhang, Z., Li, C., Hu, F., Zhang, W., Liu, Y., Zeng, Y., and Wang, J.: Low molecular weight-PAHs induced inflammation in A549 cells by activating PI3K/AKT and NF-κB signaling pathways, Toxicology Research, 10, 150–157, https://doi.org/10.1093/toxres/tfaa105, 2021.

Himona, E. and Poullikkas, A.: Comparative review of natural gas vehicles during the energy transition, Energies, 18, 3512, https://doi.org/10.3390/en18133512, 2025.

Hornung, V., Bauernfeind, F., Halle, A., Samstad, E. O., Kono, H., Rock, K. L., Fitzgerald, K. A., and Latz, E.: Silica crystals and aluminum salts activate the NALP3 inflammasome through phagosomal destabilization, Nature Immunology, 9, 847–856, https://doi.org/10.1038/ni.1631, 2008.

Huang, W., Zhang, Z., Qiu, Y., Gao, Y., Fan, Y., Wang, Q., and Zhou, Q.: NLRP3 inflammasome activation in response to metals, Frontiers in Immunology, 14, 1055788, https://doi.org/10.3389/fimmu.2023.1055788, 2023.

Jalava, P. I., Aakko-Saksa, P., Murtonen, T., Happo, M. S., Markkanen, A., Yli-Pirilä, P., Hakulinen, P., Hillamo, R., Mäki-Paakkanen, J., Salonen, R. O., Jokiniemi, J., and Hirvonen, M.-R.: Toxicological properties of emission particles from heavy duty engines powered by conventional and bio-based diesel fuels and compressed natural gas, Particle and Fibre Toxicology, 9, 37, https://doi.org/10.1186/1743-8977-9-37, 2012.

Jayaratne, E. R., He, C., Ristovski, Z. D., Morawska, L., and Johnson, G. R.: A comparative investigation of ultrafine particle number and mass emissions from a fleet of on-road diesel and CNG buses, Environmental Science & Technology, 42, 6736–6742, https://doi.org/10.1021/es800394x, 2008.

Juárez-Facio, A. T., Introna, M., Gustavsson, S. Å., Attergren, M., Lindwall, M., Olofsson, U., Steimer, S. S., and Elihn, K.: A mobile air-liquid interface exposure system optimized for outdoor toxicity testing of aerosols, Aerosol Science and Technology, 59, 214–226, https://doi.org/10.1080/02786826.2024.2426487, 2025.

Karthikeyan, S., Thomson, E. M., Kumarathasan, P., Guénette, J., Rosenblatt, D., Chan, T., Rideout, G., and Vincent, R.: Nitrogen dioxide and ultrafine particles dominate the biological effects of inhaled diesel exhaust treated by a catalyzed diesel particulate filter, Toxicological Sciences, 135, 437–450, https://doi.org/10.1093/toxsci/kft162, 2013.

Kęska, A.: The actual toxicity of engine exhaust gases emitted from vehicles: The development and perspectives of biological and chemical measurement methods, ACS Omega, 8, 24718–24726, https://doi.org/10.1021/acsomega.3c02171, 2023.

Kontses, A., Triantafyllopoulos, G., Ntziachristos, L., and Samaras, Z.: Particle number (PN) emissions from gasoline, diesel, LPG, CNG and hybrid-electric light-duty vehicles under real-world driving conditions, Atmospheric Environment, 222, 117126, https://doi.org/10.1016/j.atmosenv.2019.117126, 2020.

https://doi.org/10.5194/ar-2026-19
Preprint. Discussion started: 3 June 2026

Kwon, H.-S., Ryu, M. H., and Carlsten, C.: Ultrafine particles: Unique physicochemical properties relevant to health and disease, Experimental & Molecular Medicine, 52, 318–328, https://doi.org/10.1038/s12276-020-0405-1, 2020.

Lähde, T. and Giechaskiel, B.: Particle number emissions of gasoline, compressed natural gas (CNG) and liquefied petroleum gas (LPG) fueled vehicles at different ambient temperatures, Atmosphere, 12, 893, https://doi.org/10.3390/atmos12070893, 2021.

Latvala, S., Hedberg, J., Möller, L., Odnevall Wallinder, I., Karlsson, H. L., and Elihn, K.: Optimization of an air-liquid interface exposure system for assessing toxicity of airborne nanoparticles, Journal of Applied Toxicology, 36, 1294–1301, https://doi.org/10.1002/jat.3304, 2016.

Latvala, S., Vare, D., Karlsson, H. L., and Elihn, K.: In vitro genotoxicity of airborne Ni-NP in air–liquid interface, Journal of Applied Toxicology, 37, 1420–1427, https://doi.org/10.1002/jat.3510, 2017.

Li, Y., Xue, J., Peppers, J., Kado, N. Y., Vogel, C. F. A., Alaimo, C. P., Green, P. G., Zhang, R., Jenkins, B. M., Kim, M., Young, T. M., and Kleeman, M. J.: Chemical and toxicological properties of emissions from a light-duty compressed natural gas vehicle fueled with renewable natural gas, Environmental Science & Technology, 55, 2820–2830, https://doi.org/10.1021/acs.est.0c04962, 2021.

Lin, S., Ryan, I., Paul, S., Deng, X., Zhang, W., Luo, G., Dong, G.-H., Nair, A., and Yu, F.: Particle surface area, ultrafine particle number concentration, and cardiovascular hospitalizations, Environmental Pollution, 310, 119795, https://doi.org/10.1016/j.envpol.2022.119795, 2022.

Lv, Z., Wu, L., Ma, C., Sun, L., Peng, J., Yang, L., Wei, N., Zhang, Q., and Mao, H.: Comparison of CO2, NOx, and VOCs emissions between CNG and E10 fueled light-duty vehicles, Science of the Total Environment, 858, 159966, https://doi.org/10.1016/j.scitotenv.2022.159966, 2023.

Maikawa, C. L., Zimmerman, N., Rais, K., Shah, M., Hawley, B., Pant, P., Jeong, C.-H., Delgado-Saborit, J. M., Volckens, J., Evans, G., Wallace, J. S., and Godri Pollitt, K. J.: Murine precision-cut lung slices exhibit acute responses following exposure to gasoline direct injection engine emissions, Science of the Total Environment, 568, 1102–1109, https://doi.org/10.1016/j.scitotenv.2016.06.173, 2016.

Malakar, A., Kanel, S. R., Ray, C., Snow, D. D., and Nadagouda, M. N.: Nanomaterials in the environment, human exposure pathway, and health effects: A review, Science of the Total Environment, 759, 143470, https://doi.org/10.1016/j.scitotenv.2020.143470, 2021.

Moreno-Ríos, A. L., Tejeda-Benítez, L. P., and Bustillo-Lecompte, C. F.: Sources, characteristics, toxicity, and control of ultrafine particles: An overview, Geoscience Frontiers, 13, 101147, https://doi.org/10.1016/j.gsf.2021.101147, 2022.

Øvrevik, J., Refsnes, M., Låg, M., Holme, J., and Schwarze, P.: Activation of proinflammatory responses in cells of the airway mucosa by particulate matter: Oxidant- and non-oxidant-mediated triggering mechanisms, Biomolecules, 5, 1399–1440, https://doi.org/10.3390/biom5031399, 2015.

https://doi.org/10.5194/ar-2026-19
Preprint. Discussion started: 3 June 2026

Pino, J. S., Alvarado, P. N., Larrea, A. M., Rojas, W., and Gomez-Lopera, N.: Analysis of cytotoxicity and genotoxicity of diesel exhaust PM2.5 generated from diesel and dual natural gas-diesel engines, Environmental Toxicology and Pharmacology, 114, 104638, https://doi.org/10.1016/j.etap.2025.104638, 2025.

Portugal, J., Bedia, C., Amato, F., Juárez-Facio, A. T., Stamatiou, R., Lazou, A., Campiglio, C. E., Elihn, K., and Piña, B.: Toxicity of airborne nanoparticles: Facts and challenges, Environment International, 190, 108889, https://doi.org/10.1016/j.envint.2024.108889, 2024.

Quiros, D. C., Thiruvengadam, A., Pradhan, S., Besch, M., Thiruvengadam, P., Demirgok, B., Carder, D., Oshinuga, A., Huai, T., and Hu, S.: Real-world emissions from modern heavy-duty diesel, natural gas, and hybrid diesel trucks operating along major California freight corridors, Emission Control Science and Technology, 2, 156–172, https://doi.org/10.1007/s40825-016-0044-0, 2016.

Rašić, D., Rodman Oprešnik, S., Seljak, T., Vihar, R., Baškovič, U. Ž., Wechtersbach, T., and Katrašnik, T.: RDE-based assessment of a factory bi-fuel CNG/gasoline light-duty vehicle, Atmospheric Environment, 167, 523–541, https://doi.org/10.1016/j.atmosenv.2017.08.055, 2017.

Rossner, P., Cervena, T., and Vojtisek-Lom, M.: In vitro exposure to complete engine emissions – a mini-review, Toxicology, 462, 152953, https://doi.org/10.1016/j.tox.2021.152953, 2021.

Schraufnagel, D. E.: The health effects of ultrafine particles, Experimental & Molecular Medicine, 52, 311–317, https://doi.org/10.1038/s12276-020-0403-3, 2020.

Seagrave, J., Gigliotti, A., McDonald, J. D., Seilkop, S. K., Whitney, K. A., Zielinska, B., and Mauderly, J. L.: Composition, toxicity, and mutagenicity of particulate and semivolatile emissions from heavy-duty compressed natural gas-powered vehicles, Toxicological Sciences, 87, 232–241, https://doi.org/10.1093/toxsci/kfi230, 2005.

Shahzadi, C., Di Serafino, A., Aruffo, E., Mascitelli, A., and Di Carlo, P.: A549 as an in vitro model to evaluate the impact of microplastics in the air, Biology, 12, 1243, https://doi.org/10.3390/biology12091243, 2023.

Su, W.-C., Lee, J., Afshar, M., Zhang, K., and Han, I.: Assessing community health risks from exposure to ultrafine particles containing transition metals in the Greater Houston Area, Science of the Total Environment, 912, 169067, https://doi.org/10.1016/j.scitotenv.2023.169067, 2024.

Sundermann, A., Kögel, M., and Gerlach, O.: Exhaust purification of stoichiometric natural gas applications – A screening study on the impact of catalyst composition, reaction conditions and transient effects, Applied Catalysis O: Open, 195, 207007, https://doi.org/10.1016/j.apcato.2024.207007, 2024.

Takeshita, T.: Assessing the co-benefits of CO2 mitigation on air pollutants emissions from road vehicles, Applied Energy, 97, 225–237, https://doi.org/10.1016/j.apenergy.2011.12.029, 2012.

Toumasatos, Z., Kontses, A., Doulgeris, S., Samaras, Z., and Ntziachristos, L.: Particle emissions measurements on CNG vehicles focusing on sub-23 nm, Aerosol Science and Technology, 55, 182–193, https://doi.org/10.1080/02786826.2020.1830942, 2021.

https://doi.org/10.5194/ar-2026-19
Preprint. Discussion started: 3 June 2026

Tsakonas, G., Stamatiou, R., Vouitsis, I., Sainidis, C., Facio, A. T. J., Introna, M., Steimer, S., Elihn, K., Besis, A., Kouras, A., Samara, C., Lazou, A., and Samaras, Z.: Diesel particle filter regeneration: Impact on the physicochemical composition and toxicity of diesel exhaust emissions, Science of the Total Environment, 1009, 181099, https://doi.org/10.1016/j.scitotenv.2025.181099, 2025.

Turrio-Baldassarri, L., Battistelli, C., Conti, L., Crebelli, R., Deberardis, B., Iamiceli, A., Gambino, M., and Iannaccone, S.: Evaluation of emission toxicity of urban bus engines: Compressed natural gas and comparison with liquid fuels, Science of the Total Environment, 355, 64–77, https://doi.org/10.1016/j.scitotenv.2005.02.037, 2006.

Tzamkiozis, T., Stoeger, T., Cheung, K., Ntziachristos, L., Sioutas, C., and Samaras, Z.: Monitoring the inflammatory potential of exhaust particles from passenger cars in mice, Inhalation Toxicology, 22, 59–69, https://doi.org/10.3109/08958378.2010.519408, 2010.

Vallabani, N. V. S., Gruzieva, O., Elihn, K., Juárez Facio, A., Steimer, S., Kuhn, J., Silvergren, S., Portugal, J., Piña, B., Olofsson, U., Johansson, C., and Karlsson, H.: Toxicity and health effects of ultrafine particles: Towards an understanding of the relative impacts of different transport modes, Environmental Research, 231, 116186, https://doi.org/10.1016/j.envres.2023.116186, 2023.

Vouitsis, I., Portugal, J., Kontses, A., Karlsson, H. L., Faria, M., Elihn, K., Juárez-Facio, A. T., Amato, F., Piña, B., and Samaras, Z.: Transport-related airborne nanoparticles: Sources, different aerosol modes, and their toxicity, Atmospheric Environment, 301, 119698, https://doi.org/10.1016/j.atmosenv.2023.119698, 2023.

Weitekamp, C. A., Kerr, L. B., Dishaw, L., Nichols, J., Lein, M., and Stewart, M. J.: A systematic review of the health effects associated with the inhalation of particle-filtered and whole diesel exhaust, Inhalation Toxicology, 32, 1–13, https://doi.org/10.1080/08958378.2020.1725187, 2020.

Xue, J., Li, Y., Peppers, J., Wan, C., Kado, N. Y., Green, P. G., Young, T. M., and Kleeman, M. J.: Ultrafine particle emissions from natural gas, biogas, and biomethane combustion, Environmental Science & Technology, 52, 13619–13628, https://doi.org/10.1021/acs.est.8b04170, 2018.

Yang, H.-H., Chien, S.-M., Chao, M.-R., and Lin, C.-C.: Particle size distribution of polycyclic aromatic hydrocarbons in motorcycle exhaust emissions, Journal of Hazardous Materials, 125, 154–159, https://doi.org/10.1016/j.jhazmat.2005.05.019, 2005.